RESEARCH ARTICLE | FEBRUARY 21 2024

A computational model of the human colon for use in medical robotics

M. Evans 🕶 📵 ; S. Dogramadzi 📵



AIP Advances 14, 025244 (2024) https://doi.org/10.1063/5.0179544





Articles You May Be Interested In

The role of geometry in the friction generated on the colonic surface by mucoadhesive films J. Appl. Phys. (July 2006)

Drug delivering strategies for colon targeting in IBD treatment: A comprehensive review *AIP Conf. Proc.* (October 2024)

An extensive examination of gastrointestinal abnormalities utilizing endoscopic imaging and deep learning AIP Conf. Proc. (July 2025)





A computational model of the human colon for use in medical robotics

Cite as: AIP Advances 14, 025244 (2024); doi: 10.1063/5.0179544 Submitted: 20 October 2023 • Accepted: 29 January 2024 • Published Online: 21 February 2024







M. Evans^{a)} D and S. Dogramadzi^{b)}



AFFILIATIONS

Department of Automatic Control and Systems Engineering, The University of Sheffield, Sheffield, South Yorkshire S10 2TN, United Kingdom

a) Author to whom correspondence should be addressed: maevans1@sheffield.ac.uk

b) Email: s.dogramadzi@sheffield.ac.uk

ABSTRACT

This paper reports on the results of modeling the human colon and analyzes its effectiveness as a finite element analysis (FEA) tool for testing conventional and robotic colonoscope technologies. FEA has been used to model colon tissue before, but these analyses have been carried out on smaller tissue samples, such as to fit strain energy functions to mechanical testing data or to explore the inflation-extension response of a section of the colon. The full colon has not yet been modeled in this way, and this study aims to show the usefulness of such a tool for testing endoscopic devices for diagnostic and therapeutic purposes in the colon. Data from the literature and databases have been used to approximate the stress response of the tissues, and a critical analysis of the limitations of the approximations has been carried out. Characteristic colonoscope loops were created to analyze the mechanical response of the colon and provide comparable results to conventional colonoscopy. The results showed how stress would be propagated along the length of the colon and how neighboring structures can affect the stresses and strains experienced by the colon wall, demonstrating the need for and capabilities of a full FEA model of the colon to test endoscopic devices.

© 2024 Author(s). All article content, except where otherwise noted, is licensed under a Creative Commons Attribution (CC BY) license (http://creativecommons.org/licenses/by/4.0/). https://doi.org/10.1063/5.0179544

I. INTRODUCTION

Worldwide, colorectal cancer (CRC), a group term for cancers of the colon, rectum, or anus, is the third highest cancer type for incidence (10.2%) and the second highest type for mortality (9.2%).1 A 2020 study showed that there were an estimated 1.9×10^6 instances of CRC, resulting in 0.9×10^6 deaths worldwide.2 The study also uses current trends to predict that by 2040, the global CRC incidence rate will have risen to 3.2×10^6 . Other diseases affecting the colon include diverticulitis, irritable bowel syndrome (IBS), Crohn's disease/ulcerative colitis (inflammatory bowel diseases), clostridium difficile infection (C-diff), and

Colonoscopy is a technique that is used in the diagnosis of all of these diseases, and as of 2015, it was the leading method for evaluating positive CRC results. This procedure also allows practitioners to remove bowel polyps, thereby being able to treat and reduce the risk of CRC.4 During a colonoscopy, a gastroenterologist will insert an endoscope (a colonoscope for this practice) into a patient's colon via

the anus. The colonoscope is equipped with fiber optics, allowing for a light source and camera to view the inside of the patient's colon.

Some factors that may impede the screening of colonoscopy were identified in an academic review from 2020, including excessive costs, lack of validated competency assessment tools during training, patient's views on the procedure, and their preference for non-invasive options such as computed tomography (CT) scans.⁵

While flexible colonoscopy is the gold standard method for CRC screening, robotic technologies have been in development since the 1990s, with inchworm-like devices.⁵⁻⁷ Wireless capsule endoscopic devices have been designed to capture images from the small intestine (due to a lack of ability for this with conventional colonoscopes).8

Current testing methods for new endoscopic devices include polystyrene test beds containing ex vivo colon tissue^{6,7} and in vivo pig models^{7,9} where the device is tested in an anesthetized pig that is killed post-examination to check for damage to the colon and for clinical trials to test feasibility in human volunteers.9 A computational model with which to test new devices digitally could create an

environment with conditions closer to an in-vivo human colon than polystyrene test beds and negate the need for animal testing.

Thus, with the increased development of robotic colonoscopes, there is a need for a computational model of the colon to simulate the stress that novel devices exert on the colon wall, and while colon wall tissue has been modeled numerically and computationally in the past, ^{10–14} there is still no full model of the large intestine that can be used for this kind of analysis. This report begins to investigate the capabilities of such a model, such as calculating the stress experienced along the colon from a stimulus at one point, and the limitations to overcome to create a valid working simulation, such as material models, neighboring structures, and points of support at the colon walls.

II. METHODS

A. Geometry

Images from a CT colonography scan (from the Cancer Imaging Archives) were used to segment the geometry of the colon lumen in the open-source software ITK-Snap (Fig. 1). Using this shape, simplified geometry was created (Fig. 2) by extruding concentric rings into cylinder approximations. The lumen diameter was used to estimate the wall thicknesses throughout the colon, based on a study exploring the relationship between lumen diameter and wall thickness across 100 human subjects¹⁵ (see Table I). This was done due to the thickness of the wall affecting local stress/strain responses in the wall, with thicker-walled areas such as the sigmoid colon being less compliant than thinner-walled areas such as the ascending colon.

Using this simplification, the haustra, folds, and tenia coli were omitted from the model. The ileocecal valve and anal sphincter were modeled as small circular openings, with locations based on the CT colonography and fixed constraints applied. Fixed constraints were applied to the hepatic and splenic flexures (as these sections are much more fixed than others ¹⁶), and elastic constraints were

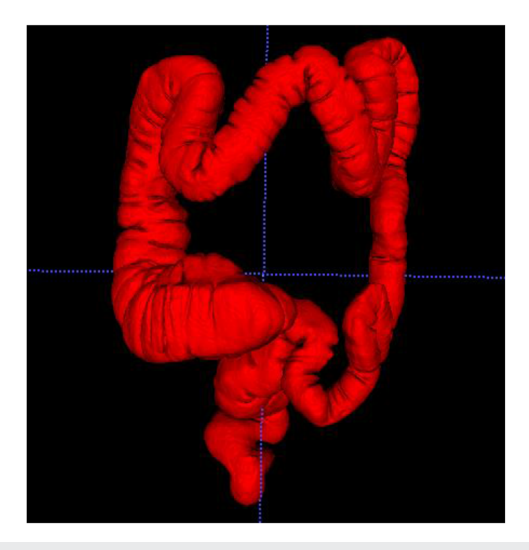


FIG. 1. Segmented geometry of the colon, completed using the CT colonography scan in ITK-Snap.

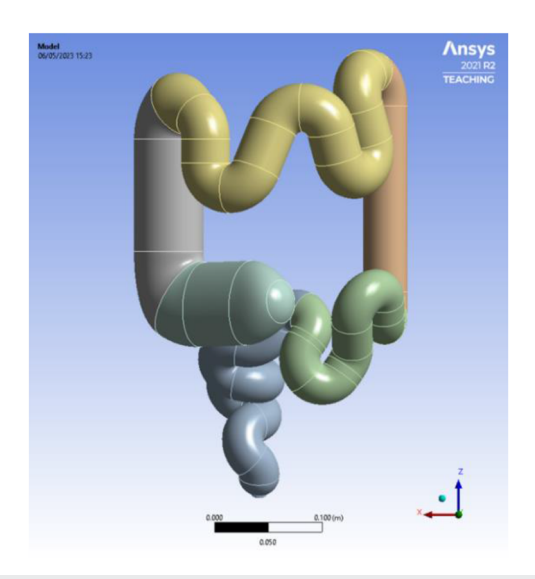


FIG. 2. Full simplified geometry of the colon, with different sections represented by different colors.

applied to simulate the interactions with the mesocolon and rectal muscles.

B. Materials

Physical properties were approximated to relieve the computational burden, but at the cost of accuracy. Values for the colon wall were estimated using a mechanical study report, ¹⁷ using the elastic modulus, yield strength, and ultimate tensile strength (UTS) to approximate a linear, isotropic response to relieve the computational burden. Due to the anisotropic nature of the colon wall, longitudinal and circumferential elastic responses were different, ¹⁷ so the value for Young's modulus for each area was the mean average of the two, and the values for yield strength and UTS were chosen to be the lower of each directional response, so as not to predict failure at higher stress than measured experimentally.

Previous studies have modeled the biphasic response, ^{17,18} multilayer composition, ^{10,11} and non-linear hyperelasticity; ^{12–14} however, these were all either mathematical models or computational models on a much smaller sample of tissue. As the whole colon has been modeled in this study, modeling these properties would take a large amount of time and computational resources. Limitations arising from this will be discussed in Sec. IV C.

TABLE I. List of the geometrical properties of the simplified model for each section. 15

Location	Lumen Ø (mm)	Wall thickness (mm)		
Cecum	80 × 60	2		
Ascending	60	2		
Transverse	40	2.5		
Descending	35	3		
Sigmoid	30	4		
Rectum	30	4		

TABLE II. Material properties of the different sections of the colon based on results from the literature. 17

Section material	Young's modulus (MPa)	Yield strength (MPa)	Ultimate tensile strength (MPa)
Ascending	4.24	0.53	0.71
Transverse	3.18	0.3	0.77
Descending	2.5	0.35	0.6
Sigmoid	2.66	0.4	0.72

The properties of the materials created for the colon wall are given in Table II. The cecum used the ascending wall properties, and the rectum used the sigmoid wall properties. Surrounding structures were modeled as simple elastic constraints, ^{19,20} as they were still relevant but less important to measure for this project—the colon wall/device interaction was the desired response.

C. Meshing

An n-loop scenario was created with a colonoscope contact model in the sigmoid area of the colon model. The distal end of the "scope" was fixed, and the proximal end was displaced 4 cm down the axis of the colon. This allowed mesh independence to be measured with relevant metrics of stress and displacement.

The mesh size began at an element size of 7 mm and was initially decreased in increments of 1 mm, then 0.1 mm when this increment became too high.

D. Material validation

A mechanical testing study²¹ was used to validate the materials created for the colon wall. Three orientations of the colon tip were modeled: a 0° bend (I), a 90° bend (L), and a 180° bend (U). The colonoscope modeled was the EVIS EXCERA CF-HQ190I/L.²²

The tip models were displaced into a circle of tissue—96 mm in diameter, with an unconstrained central 70 mm diameter area—at small time increments until the UTS¹⁷ was observed. With three orientations and four materials, 12 permutations of results were created. The force and displacement experienced by the tip model were recorded for validation.

E. Full model demonstration

The three orientations of the scope tip were each used in the ascending, transverse, descending, and sigmoid areas of the model. Due to the different geometry from the material validation tests, it was hypothesized that a greater force would be experienced by the scope tip, as there is more area of the colon to distribute stress across before the material fails. The displacement was also expected to be higher at the UTS point of the material due to the increased area.

III. RESULTS

A. Mesh convergence

The metric used when determining convergence was the principal stress at the wall at the mean average value and 95th percentile

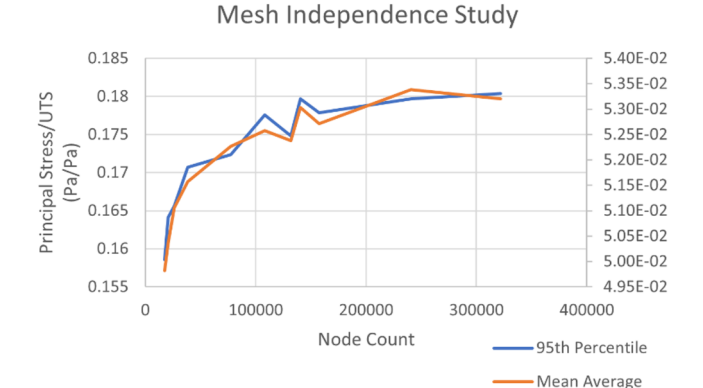


FIG. 3. Mesh convergence via principal stress at the 95th percentile (left axis) and mean average (right axis) values.

(Fig. 3) to disregard outlying values. Twelve element sizes were used from 7 to 1.4 mm.

Below 2 mm, mesh densities were localized to the area of interest, and the node count used to display results was scaled according to the mesh size at the interaction point. The element size at the wall was 1 mm to allow for multiple elements across the width of the wall.

1.5 mm was chosen as the final element size, with the size increasing by 0.5 mm at each section away from the section of interest, up to a maximum of 3 mm. Between 2.1 and 1.5 mm, the stress only changed by 0.33% (mean)/0.38% (P95), with no higher than a 1.3% difference between steps.

B. Material validation results

The summarized results from the material validation tests are presented in Table III. All materials failed at lower force and displacement levels than the porcine descending colon from the physical tests;²¹ however, the force/displacement response exhibited a close relationship to the physical response curves at the values recorded.

The tissue failed at the lowest force/displacement during the L-orientation testing and at the highest force/displacement during the U-orientation testing. This differs from the physical test results, where the L-orientation testing saw the highest force at perforation.²¹

C. Full model results

The summarized results from the tests on the full model can be seen in Table III. In all four sections, the I-orientation sub-steps converged beyond the UTS of the material and provided a valid set of results. For the L- and U- orientation tests at the ascending colon, the sub-steps of the analysis did not converge beyond the UTS, meaning that the results for the UTS were extrapolated.

The force applied to one point in the full model induced stresses throughout the section of the colon, not just localized to the point of contact. This can be seen in Fig. 4, where the stress is propagated along the length of the transverse colon. While there are stress concentrations due to harsh constraints on the model, these stresses

TABLE III. Results from the material validation and full model tests. Boldface denotes the average values for each 'colonoscope tip' orientation.

		Material validation		Full model test	
Colonoscope tip orientation	Location	Force at UTS (N)	Maximum displacement (mm)	Force at UTS (N)	Maximum displacement (mm)
I	Ascending	10.0	9.60	8.61	9.50
	Transverse	12.8	12.2	20.7	10.9
	Descending	9.94	12.1	13.1	16.8
	Sigmoid	12.6	13.1	33.1	14.8
	Average (I)	11.3	11.8	18.9	13.0
L	Ascending	2.26	3.97	15.4	14.4
	Transverse	3.93	5.86	15.0	24.6
	Descending	3.03	5.81	13.5	41.9
	Sigmoid	4.09	6.49	42.0	23.3
	Average (L)	3.3	5.5	23.5	26.1
U	Ascending	9.11	11.0	32.5	13.0
	Transverse	19.1	14.6	13.9	24.9
	Descending	15.6	15.6	19.6	21.6
	Sigmoid	22.6	17.3	19.7	42.9
	Average (U)	16.6	14.6	17.7	29.8

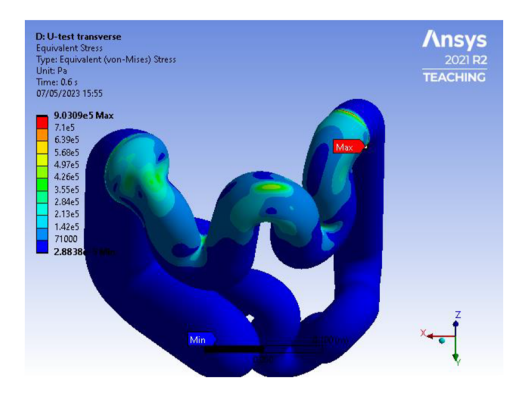


FIG. 4. U-orientation tip has been forced down into the lower left flexure of the transverse colon. This has induced stress across the whole length of the transverse colon but has also induced a stress artifact at the splenic flexure due to a harsh constraint placed on the splenic flexure.

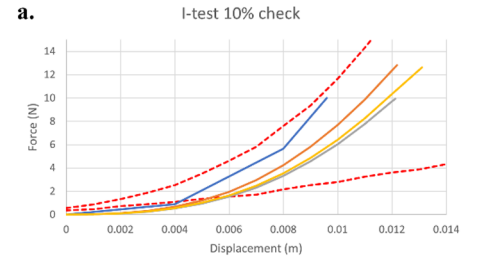
would be propagated further past these boundaries in a model with improved constraints.

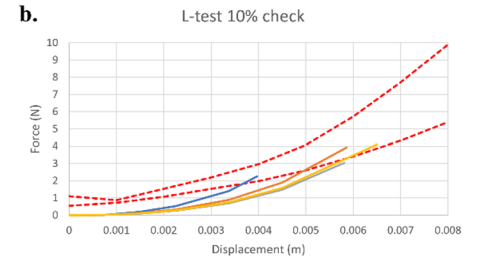
IV. DISCUSSION

A. Material validation

The material response was aimed at finding results within 10% of the upper and lower limits of the data from the recreated mechanical test.²¹ A graphical representation of this target can be seen in Fig. 5.

The calculated force/displacement response followed the general trend of the mechanical test results, ²¹ with most calculated data points falling within 10% of the I-orientation mechanical results, but the L- and U-orientation calculated trendlines had lower force values than the mechanical results. ²¹ Looking at the red lines in Fig. 5, the





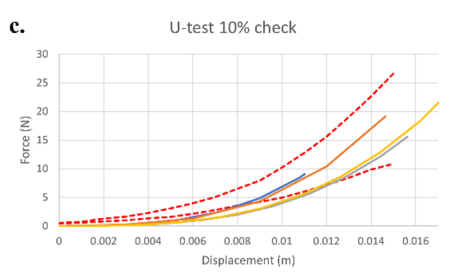
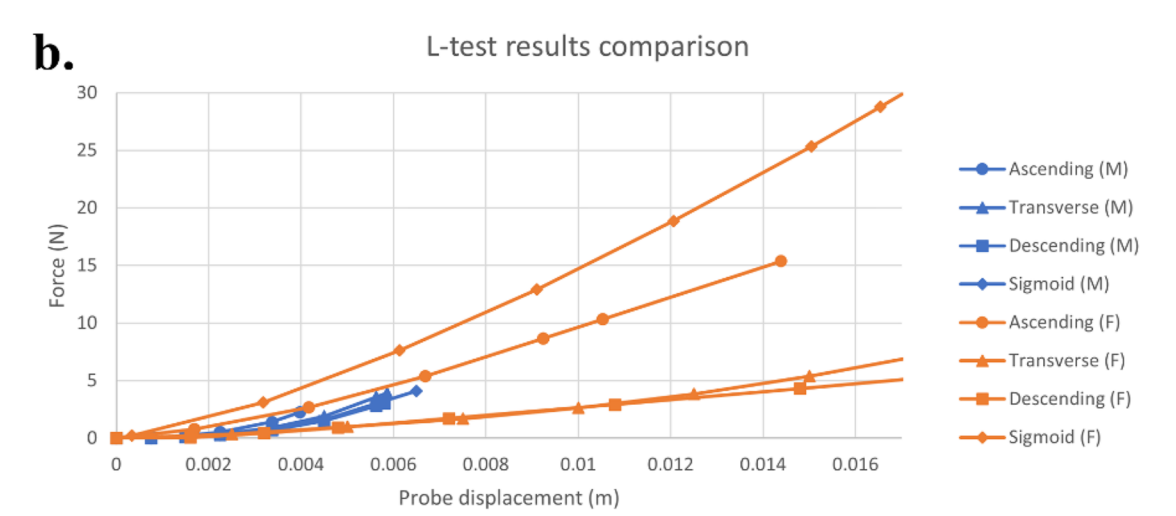


FIG. 5. Range within $\pm 10\%$ of the data points²¹ (red dash lines) and the response from the I-tests (a), L-tests (b), and U-tests (c) for the ascending (blue), transverse (orange), descending (gray), and sigmoid (yellow) material validation tests.





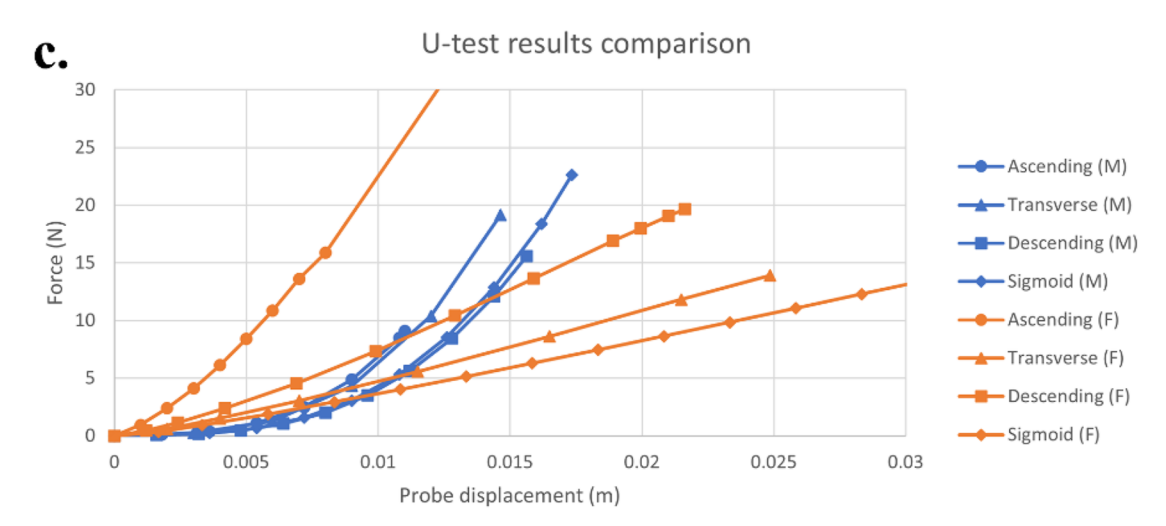


FIG. 6. Comparison between the results from the material validation tests (blue) and the full model tests (orange) for the I-shaped tip (a), L-shaped tip (b), and U-shaped tip (c). The full model tests mostly have higher force and displacement at the UTS point of the materials than seen in the material validation tests.

physical mechanical responses seem to start at a higher force than zero, which could be the issue.

The main inaccuracy was at the failure point. All materials "failed" at lower values than expected, likely due to the approximations of elastic properties used for the materials. On average, I-orientation calculations were 49% lower for displacement and 51% lower for force. L-orientation calculations were especially low, at 71% for displacement and 88% for force. U-orientation calculations were slightly better, at 38% lower for displacement and 41% lower for force on average.

It is probable that the exceptionally low failure values for the L-orientation tests were due to the recreation of the L-orientation tip geometry. The length of the tip was close to the diameter of unconstrained tissue material, creating an abnormally high stress concentration at the edge of the constraint.

B. Full model

The results from the full model were compared with the results from the material validation, as the materials were the same as the computational testing, not the mechanical testing.²¹

Graphical comparisons of the results can be seen in Fig. 6, and in each instance, the force and displacement of the full model tests mostly surpass those of the material validation tests at failure. This was expected, as there was more material to be displaced and more material over which stress could be distributed, leading to higher forces experienced by the scope tip at failure.

The difference in results between a small sample of a material and the material in a model of the entire colon suggests that smaller samples of the colon may not be accurate for testing endoscopic devices. The shape and neighboring structures of the colon.

C. Limitations

Limitations arose from the simplifications and assumptions used in this project. Haustra, semilunar folds, and tenia *coli* were all omitted due to the simplified geometry used to gather data within the timeframe of the project. In reality, these would all have some effect on the response of the colon tissue to internal devices, for example, the tenia *coli*, which provides increased elastic resistance in the longitudinal direction of the colon.

The non-linear properties of the colon wall tissue were also omitted—a Hookean response was estimated from mechanical test data on porcine colon tissue.¹⁷ This will have significantly affected the realism of the model; however, there can still be a fair comparison between the material validation tests and the full model tests, as both used the same materials. This limitation affects the accuracy of the model, but the full model still shows major differences in material validation, cementing its usefulness when fewer assumptions are used.

Material failure in these analyses was determined by the point at which the UTS was reached. In the compared mechanical study, ²¹ failure was determined as when the material was fully perforated. As the colon wall is made up of multiple different layers with different stress responses, ^{10,11,13} the UTS of one layer could be reached before the wall is perforated, with other layers staying intact. Furthermore, the wall may reach a UTS and begin to take damage, with more

stress needed to damage the wall enough for perforation. One of the more impactful limitations was the arbitrary placement of constraints. The constraints were placed to mimic how the colon is connected to its neighboring structures—specifically the mesocolon and abdominal walls. As the splenic and hepatic flexures were reportedly relatively fixed areas of the colon, fixed constraints were applied to the outer walls of these areas, causing stress concentrations at the constraint boundaries that would not be seen in a colon in vivo.

V. FUTURE WORK

This work is being continued as a postgraduate research project. The tissue modeling will be improved using strain energy functions (SEFs) to consider non-linear and anisotropic hyperelasticity. ^{12–14} Starting at smaller scales and building up to a full model will allow for a manageable computational burden while applying more accuracy to the model.

The geometry will be improved by keeping the characteristic features of the colon present, such as haustra, and modeling tenia *coli* and their effects on longitudinal strain. It may be possible to look at the way different tissues and structures are connected by using a different imaging modality than CT, such as MRI. This would allow for more accurate constraints to be placed on the model, removing unrealistic stress concentrations (Fig. 4).

VI. CONCLUSION

These new results of the colon model are promising, as shown by the similar trends in the mechanical recreation simulations; however, the used materials should be refined, and anisotropic elasticity must be implemented. Further exploration into the similarities and differences of colonic anatomical geometry would provide useful insight into the major trends in geometry seen across many colons (hepatic and splenic flexures, cecum shape and direction, transverse and sigmoid colon shapes, for example), which would determine the need for a patient-specific model or allow for a generalized model that is effective for all patients.

Despite these limitations, the model represents a basis from which to create a simulation of mechanical responses from the human colon *in situ* and can be improved upon to create a mode of testing devices that is useful, safe, accurate, and the first of its kind.

ACKNOWLEDGMENTS

For the purpose of open access, the author has applied for a Creative Commons (CC BY) license to any author accepted manuscript version arising. This work is licensed under CC BY 4.0. To view a copy of this license, visit http://creativecommons.org/licenses/by/4.0/. This work was funded by the University of Sheffield Institutional Open Access Fund.

AUTHOR DECLARATIONS

Conflict of Interest

The authors have no conflicts to disclose.

Ethics Approval

Ethics approval was not required.

Author Contributions

M. Evans: Investigation (lead); Methodology (lead); Writing – original draft (lead); Writing – review & editing (lead). S. Dogramadzi: Conceptualization (lead); Supervision (lead); Writing – original draft (supporting).

DATA AVAILABILITY

The data that support the findings of this study are available within the article.

REFERENCES

- ¹F. Bray, J. Ferlay, I. Soerjomataram, R. L. Siegel, L. A. Torre, and A. Jemal, "Global cancer statistics 2018: GLOBOCAN estimates of incidence and mortality worldwide for 36 cancers in 185 countries," Ca-Cancer J. Clin. **68**(6), 394–424 (2018).
- ²Y. Xi and P. Xu, "Global colorectal cancer burden in 2020 and projections to 2040," Transl. Oncol. **14**(10), 101174 (2021).
- ³D. M. Novick, A Gastroenterologist's Guide to Gut Health: Everything You Need to Know About Colonoscopy, Digestive Diseases, and Healthy Eating (Rowman & Littlefield, Lanham, MD, 2017).
- ⁴D. K. Rex *et al.*, "Quality indicators for colonoscopy," Gastrointest. Endoscopy **81**(1), 31–53 (2015).
- ⁵G. Ciuti *et al.*, "Frontiers of robotic colonoscopy: A comprehensive review of robotic colonoscopes and technologies," J. Clin. Med. 9(6), 1648 (2020).
- ⁶P. Dario, M. C. Carrozza, and A. Pietrabissa, "Development and in vitro testing of a miniature robotic system for computer-assisted colonoscopy," Comput. Aided Surg. 4(1), 1–14 (1999).
- ⁷B. Kim, H. Y. Lim, J. H. Park, and J. O. Park, "Inchworm-like colonoscopic robot with hollow body and steering device," JSME Int. J., Ser. C **49**(1), 205–212 (2006).

 ⁸D. Cater, A. Vyas, and D. Vyas, "Robotics in colonoscopy," Am. J. Rob. Surg. **1**(1), 48–54 (2014).

- ⁹T. Rösch *et al.*, "A motor-driven single-use colonoscope controlled with a handheld device: A feasibility study in volunteers," Gastrointest. Endoscopy **67**(7), 1139–1146 (2008).
- ¹⁰Y. Zhao, S. Siri, B. Feng, and D. M. Pierce, "Computational modeling of mouse colorectum capturing longitudinal and through-thickness biomechanical heterogeneity," J. Mech. Behav. Biomed. Mater. 113, 104127 (2021).
- ¹¹Y. Zhao, B. Feng, and D. M. Pierce, "Predicting the micromechanics of embedded nerve fibers using a novel three-layered model of mouse distal colon and rectum," J. Mech. Behav. Biomed. Mater. **127**, 105083 (2022).
- ¹²B. Patel *et al.*, "Constitutive modeling of the passive inflation-extension behavior of the swine colon," J. Mech. Behav. Biomed. Mater. 77, 176–186 (2018).
- ¹³E. L. Carniel, V. Gramigna, C. G. Fontanella, C. Stefanini, and A. N. Natali, "Constitutive formulations for the mechanical investigation of colonic tissues," J. Biomed. Mater. Res., Part A 102(5), 1243–1254 (2013).
- ¹⁴S. Puértolas, E. Peña, A. Herrera, E. Ibarz, and L. Gracia, "A comparative study of hyperelastic constitutive models for colonic tissue fitted to multiaxial experimental testing," J. Mech. Behav. Biomed. Mater. 102, 103507 (2020).
- ¹⁵W. Wiesner, K. J. Mortelé, H. Ji, and P. R. Ros, "Normal colonic wall thickness at CT and its relation to colonic distension," J. Comput. Assisted Tomogr. **26**(1), 102–106 (2002).
- $^{16}\mathrm{M.\,L.}$ Corman, Colon and Rectal Surgery (Lippincott Williams & Wilkins, Cop., Philadelphia, 2005).
- ¹⁷D. Massalou *et al.*, "Dynamic biomechanical characterization of colon tissue according to anatomical factors," J. Biomech. **49**(16), 3861–3867 (2016).
- ¹⁸T. K. Wu, "Occult injuries during colonoscopy: Measurement of forces required to injure the colon and report of cases," Gastrointest. Endoscopy 24(5), 236–238 (1978).
- ¹⁹E. J. White, E. M. Cunnane, M. McMahon, M. T. Walsh, J. C. Coffey, and L. O'Sullivan, "Mechanical characterisation of porcine non-intestinal colorectal tissues for innovation in surgical instrument design," Proc. Inst. Mech. Eng., Part H 232(8), 796–806 (2018).
- ²⁰ K. Isogai *et al.*, "Young's moduli of subcutaneous tissues and muscles under different loads at the gluteal region calculated using ultrasonography," J. Phys. Ther. Sci. **34**(12), 777–783 (2022).
- ²¹ S. Johnson, M. Schultz, M. Scholze, T. Smith, J. Woodfield, and N. Hammer, "How much force is required to perforate a colon during colonoscopy? An experimental study," J. Mech. Behav. Biomed. Mater. **91**, 139–148 (2019).
- 22 Olympus Medical Systems, Gastroenterology Products for Gastrointestinal Endoscopy, www.olympus.co.uk, 2023, https://www.olympus.co.uk/medical/en/ products-and-solutions/medical-specialities/gastroenterology/.